Influence of a periodic magnetic field and spin-polarized current on the magnetic dynamics of a monodomain ferromagnet

Paul P. Horley,[1,2] Vítor R. Vieira,[1] Peter M. Gorley,[2] Vitalii K. Dugaev,[1,3] Jamal Berakdar,[4] and Józef Barnaś[5,*]

[1]*Department of Physics and CFIF, Instituto Superior Técnico, Universidade Técnica de Lisboa, Avenida Rovisco Pais, 1049-001 Lisboa, Portugal*

[2]*Department of Physics, Yuri Fedkovych Chernivtsi National University, 2 Kotsyubynsky Street, 58012 Chernivtsi, Ukraine*

[3]*Department of Mathematics and Applied Physics, Rzeszów University of Technology, Powstańców Warszawy 6, 35-959 Rzeszów, Poland*

[4]*Institut für Physik, Martin-Luther-Universität Halle-Wittenberg, D-06120 Halle, Germany*

[5]*Institute of Molecular Physics, Polish Academy of Sciences, Smoluchowskiego 17, 60-179 Poznań, Poland*

(Received 28 March 2008; revised manuscript received 12 June 2008; published 13 August 2008)

Motivated by numerous experiments on the magnetization reversal by electric current and magnetic-field pulses, we performed a numerical simulation within a macrospin model with periodic field and spin-polarized current, also taking into account the anisotropy of damping. It is shown that the magnetic dynamics is strongly affected by the variation of frequency and shape of the pulses. In particular, single rectangular pulses of the current can be used to achieve faster magnetization reversal, whereas harmonic alternating magnetic fields lead to magnetization precessional modes with potential technological applications. The use of rectangular field pulses allows generation of several important oscillation modes at lower fields, although the resulting magnetization dynamics turned out to be rather noisy.

DOI: 10.1103/PhysRevB.78.054417 PACS number(s): 75.50.Cc, 75.30.Gw, 75.40.Mg, 85.75.−d

I. INTRODUCTION

The efficient use of the quickly developing technology of nonvolatile magnetic memories (MRAM) requires a detailed understanding of the magnetization dynamics in nanometer-thick magnetic films. One of the most important problems of MRAM technological applications is related to the efficient control of the magnetization dynamics to achieve the fastest magnetization reversal under relatively small fields and currents. At the same time, special attention is paid to the anticipated spin valve applications for the generation of magnetization oscillations of gigahertz frequencies.[1–6]

The simplest spin valve, revealing the giant magnetoresistance (GMR) effect, is composed of two magnetic layers separated by a nonmagnetic spacer.[7] One of the magnetic layers is thicker than the other one and acts as a polarizer of the current, orienting the spins of the electrons in the same direction. The other magnetic layer, which is very sensitive to the applied field and to the spin torque rendered by the incoming flux of spin-polarized carriers, is called "analyzer." In the minimal model, it can be treated as a Stoner-Wohlfarth particle[8] and is usually described in the framework of the macrospin approximation[9,10] of the Landau-Lifshitz-Gilbert (LLG) theory.

There are several well-known limitations of the macrospin approximation. Describing the magnetic particle as a macroscopic magnetic moment, one assumes that the magnitude of this moment is constant. It should be noted that this condition does not necessarily require homogeneity of the magnetization. However, it is obvious that the macrospin model describes correctly the dynamics of a single-domain magnetic particle. The other assumption concerns the effect of a spin-polarized current acting on the magnetic moment in the frame of the macrospin model. This current is included in the LLG model of magnetic dynamics in a way that its transverse part is completely absorbed within the magnetic particle. It means that, in the general case, it may differ from the spin current in a polarizer and has to be found from the equations describing the spin transport in the multilayer system. Nevertheless, it was shown that the LLG model is capable of displaying characteristic types of the magnetization motion observed experimentally, such as magnetization reversal,[8,11] relaxation of the magnetization vector to an intermediate canted state,[12] and two types of steady precession taking place roughly in the easy magnetization plane (IPP, in-plane precession) and outside of the latter (OPP, out-of-plane precession).[2,9,10]

The question of prime concern for the design of magnetic memory chips is connected with efficient and quick magnetization reversal. In the general case, this task implies device optimization over the magnitude and mutual orientation of external magnetic field and spin current polarization vector. The experimental studies[1–3] revealed that the application of a constant magnetic field or the injection of a dc spin current allows to obtain magnetization reversal times within nanoseconds.[13–15] Such high values are caused by the magnetization "ringing" phenomenon, when the macrospin performs a small-angle precession during its relaxation toward the corresponding stationary state. Ringing can occur both in the vicinity of the easy plane[16] or cover the entire unitary sphere.[17,18] Use of ac currents[19] and fields allows to suppress the ringing in different degrees, thus achieving magnetization switching on the timescale of dozens of picoseconds.[20–22] The macrospin switching along the shortest trajectory, so-called "ballistic[23] magnetization reversal" (BMR), in the ideal case takes place along a meridian of the unitary sphere. To force a macrospin doing this type of switching, one should use a properly timed current "chirp" to trigger the desired wide-angle precession.[24,25] To achieve the best results, the series of current pulses should be dynamically tuned with the oscillation frequency of the macrospin.[26,27] If the reversal is achieved by means of a magnetic field, the

latter should be switched off at the moment when the sign of a magnetization component changes.[28] This method enables to perform the reversal by a single pulse, but requires high timing precision, since otherwise the moment may flip back to the initial state.[29] Moreover, the use of alternating magnetic fields can also decrease significantly the critical field magnitude triggering the macrospin reversal, bringing it well below the magnitude of the magnetic anisotropy.[30–32]

In the case of an ac magnetic field applied along the easy axis, the reported reversal times remain at the nanosecond scale,[33] while a faster switching (hundreds of picoseconds) was confirmed experimentally for the case when the field pulse is applied in the easy magnetization plane at a certain angle,[34] sometimes almost perpendicular[20,23] to the easy axis. Another alternative of exciting magnetization precession without sophisticated field-angle tuning consists of the application of a circularly[35,36] or linearly polarized[14] field. At the same time, a proper frequency choice for the external driving force may cause synchronization of the magnetic oscillations with a microwave,[35,37] opening interesting application perspectives for GHz-frequency generators of modulated signal.

Therefore, the task of reaching the fastest magnetization reversal presents a very complicated problem requiring multidimensional optimization in the space of numerous control parameters. However, the resulting methodology should be suitable for practical realization, which, in our opinion, may address the experimentally simpler way to attain both the magnetization reversal and the synchronized oscillations with the help of the oscillating fields and/or currents, preferably without precise tuning of the signals or tracing the current polarization with respect to the magnetization. At the same time, additional control can be introduced via changing the driving force frequency and by assigning different time profiles for its pulses. First of all, the detailed investigations should be performed for the case of collinear field and current polarization, i.e., the commonly used configuration in technological devices such as hard disk read/write heads, where bits 0 and 1 correspond to opposite magnetization directions parallel to the easy axis.[38] Because of the complexity of the synchronization due to various shapes of current and field pulses, the behavior of the system can be most efficiently studied numerically. Our results confirm the possibility of magnetization reversal within hundreds of picoseconds in a wide range of the control parameters, weakening the requirements for their precise fine tuning. We found various types of the synchronized motion yielding phase portraits that are impossible to obtain under a constant field. The registered oscillation modes have characteristics that may be of interest for potential applications.

The paper is organized as follows: In Sec. II we discuss the model and calculation details. Special attention is paid to account for the magnetization damping, which is responsible for deceleration of the magnetization movement due to the dissipation of the macrospin energy. Section III presents the results concerning the influence of an alternating spin current on the macrospin dynamics compared with the constant applied field/current case. Particular emphasis is placed on the magnetization reversal phenomena triggered by the individual or multiple current pulses of varying duration. Section IV discusses the behavior of a macrospin subjected to a time-varying magnetic field, also characterized by different pulse profiles and frequencies. Section V presents the main conclusions of the paper.

II. THEORETICAL MODEL AND CALCULATION DETAILS

The magnetization dynamics of a Stoner-Wohlfarth particle is usually described by the Landau-Lifshitz-Gilbert equation (see, e.g., Ref. 4),

$$\frac{d\mathbf{M}}{dt} = -\gamma[\mathbf{M}\times\mathbf{H}] + \frac{\gamma}{M_s}[\mathbf{M}\times(\mathbf{M}\times\mathbf{J})] + \frac{\alpha}{M_s}\left[\mathbf{M}\times\frac{d\mathbf{M}}{dt}\right], \tag{1}$$

where $\mathbf{M}$ is a macrospin magnetization vector, $\mathbf{H}$ is the effective field (including the anisotropy and the demagnetizing field $\mathbf{H}_D=[0,0,-M_z]$, as well as the external applied magnetic field $\mathbf{H}_E$, which make the respective contributions to the energy density of the particle $\mathcal{E}(\mathbf{M},\mathbf{H})=K[1-(M_x/M_s)^2]+\frac{1}{2}\mu_0\mathbf{M}\cdot\mathbf{H}_D-\mu_0\mathbf{M}\cdot\mathbf{H}_E$); $\mathbf{J}$ denotes the spin-polarization vector of the injected current, $\gamma=2.21\times10^5$ $(\mathrm{sA/m})^{-1}$ is the electron gyromagnetic ratio, and α is a phenomenological damping constant introduced by Gilbert.[39] As LLG Eq. (1) preserves the magnitude of the particle magnetization $|\mathbf{M}|=M_s$, it can be alternatively rewritten for the spherical coordinate system in terms of angles θ and φ defining the orientation of the normalized magnetization vector $\mathbf{m}=\mathbf{M}/M_s$:[38]

$$\frac{\partial\theta}{\partial\tau} = -\sin\theta(\alpha A - B), \quad \frac{\partial\varphi}{\partial\tau} = \alpha B + A, \tag{2}$$

where

$$A = Z(\varphi)\cos\theta + h(\tau), \quad B = \frac{1}{2}h_p\sin 2\varphi + h_s(\tau),$$

$$Z(\varphi) \equiv (1 + h_p\cos^2\varphi), \quad \tau = t\gamma H_k/(1+\alpha^2). \tag{3}$$

Here $h_p=K_p/K$ and $h_s=\hbar\eta J/4edSK$ are, respectively, the dimensionless easy-plane anisotropy and the spin current depending on the easy-axis and easy-plane anisotropy constants K and K_p; J/S is the current density, η is the polarization degree of the carriers, and finally, d and S represent the thickness and area of the magnetic layer, respectively. The applied field normalized to the uniaxial anisotropy $H_k=2K/M_s$ is characterized by the dimensionless parameter h and assumed collinear with the easy magnetization axis z. In our calculations we use parameters characteristic of thin cobalt layers and used in the Co/Cu/Co spin valves as reported in the experiment:[2] $\alpha_0=0.014$, $d=3$ nm, $S=130\times70$ nm^2, $K_p=10$ kOe, $H_k=500$ Oe ($h_p=20$). The time constant is $\tau_0=(1+\alpha^2)/(\gamma H_k)=110$ ps.

Equation (2) was solved using the Runge-Kutta method of the fourth order with the integration step $\tau_{\mathrm{int}}=1$ ps. For each phase portrait 35000 points of $\theta(\tau)$ and $\varphi(\tau)$ were calculated, reconstructing a three-dimensional trajectory of the magnetization vector tip according to the formulas

$$m_x = \sin\theta\cos\varphi,$$

$$m_y = \sin\theta \sin\varphi,$$

$$m_z = \cos\theta. \quad (4)$$

The stationary state of the system is characterized by four equilibrium magnetic configurations, including $\mathbf{m}=\{0,0,+1\}$ and $\mathbf{m}=\{0,0,-1\}$.[38] Therefore, the initial values of the angular variables were chosen in the vicinity of either of these points ($\varphi^0=0$, $\theta^0=0.01\pi$ or $\theta^0=0.99\pi$, respectively), which allows observation of hysteretic phenomena.[9] It was shown that in the case considered the variation of initial value of the angle φ^0 does not influence the dynamics of the system in a qualitative way.

Numerous debates in the current literature address the question of the appropriateness of using a constant Gilbert damping[39] to describe the magnetic dynamics. In general, the damping is related to the macrospin energy transfer to spin waves, lattice vibrations, etc. As both acceleration and deceleration of the magnetic motion are caused by an imbalance between the driving and damping forces, one may assume that the damping has a viscous nature, i.e., is proportional to the rate of magnetization variation.[39] For a more realistic multidomain structure one should take into account possible variations of the shape and size of the domains, which makes α vary within the particle. Even in the macrospin case, when all the subparticles comprising the magnetic body behave as a single one, general considerations require the damping coefficient to depend on internal and external parameters of the system. Several possible cases of such dependences were already discussed in the literature. In particular, Katsura *et al.*[40] showed that α changes linearly with the applied voltage in a magnetic junction. Accounting for the angular dependence of Gilbert damping coefficient on the vertical angle θ, Kim *et al.*[41] demonstrated that the damping coefficient can be twice as large as α_0 introduced by Gilbert for Py/Cu and Co/Cu interfaces. Other approaches use a dry-friction dissipation model,[33] in which the damping is expressed in terms of the scattering matrix[42] that can be calculated from first principles. The studies of the ferromagnetic resonance[43] in the range of frequencies from 1 to 225 GHz allowed separation of the viscous damping component from the dissipation caused by two-magnon interactions dominating in Fe-V sandwiches. This approach requires the inclusion of the Bloch-Bloembergen spin relaxation processes thus allowing to account for the magnetization precession energy scattering and resulting in a variable length of the magnetization vector. The influence of a spin-lattice interaction on the magnetization damping was considered in Ref. 44. Further, it was shown that both the spin pumping and the two-magnon scattering are important for the functioning of devices based on thin magnetic films.[42,43,45] It was also suggested that in the general case the magnetization damping should take into account local effects,[46] tracking the local magnetization history and thus becoming both time and coordinate dependent, which complicates the phenomenological description and the adequate models of high-frequency devices, especially at short length scales.[45]

Here we employ the approach proposed by Tiberkevich and Slavin,[47] who aimed to explain an abrupt jump of microwave frequency as a function of spin current observed in spin valves experiments. They suggested to consider the case when the isotropic energy dissipation for a macrospin depends only on its dynamical characteristics and preserve the length of the magnetization vector. Thus, the generalized magnetic torque $\mathbf{T}$ can be written in the form[47]

$$\mathbf{T} = \frac{\alpha(\xi)}{M_s}\left(\mathbf{M}\times\frac{d\mathbf{M}}{dt}\right) + \alpha'(\xi)\frac{d\mathbf{M}}{dt} + \gamma M_s \alpha''(\xi)\mathbf{M}. \quad (5)$$

In this formula, the effect of α' will be a renormalization of the gyromagnetic ratio, and for small damping it could be neglected; α'' does not preserve the length of the magnetization vector and must be set equal to zero. Therefore, we consider only the first term in Eq. (5), which is structurally similar to Gilbert damping, but includes the information on local magnetization dynamics because, as proposed by Tiberkevich and Slavin, it depends on the dimensionless variable ξ proportional to $(d\mathbf{M}/dt)^2$ with a corresponding normalization coefficient. In our case,

$$\left(\frac{d\mathbf{M}}{dt}\right)^2 = M_s^2\left[\left(\frac{\partial\theta}{\partial t}\right)^2 + \sin^2\theta\left(\frac{\partial\varphi}{\partial t}\right)^2\right], \quad (6)$$

so that using $\partial\theta/\partial\tau$ and $\partial\varphi/\partial\tau$ from Eq. (2) and the reduced time variable τ defined in Eq. (3), one will obtain

$$\left(\frac{d\mathbf{M}}{dt}\right)^2 = \frac{\gamma^2 H_k^2 M_s^2}{(1+\alpha_0^2)^2}(1+\alpha^2)(A^2+B^2)\sin^2\theta$$

$$\approx \frac{\gamma^2 H_k^2 M_s^2}{(1+\alpha_0^2)}(A^2+B^2)\sin^2\theta. \quad (7)$$

Here the relation $1+\alpha_0^2 \approx 1+\alpha^2$ was used because the expected corrections to the damping coefficient should be small with respect to the constant damping coefficient α_0. Therefore, similarly to Ref. 47, the expression for ξ can be written as

$$\xi = \frac{\alpha_0^2(1+\alpha_0^2)}{\gamma^2 H_k^2 M_s^2}\left(\frac{d\mathbf{M}}{dt}\right)^2 = \alpha_0^2(A^2+B^2)\sin^2\theta, \quad (8)$$

where α_0^2 was introduced in the nominator to make $\xi \ll 1$, enabling the Taylor expansion of the damping coefficient

$$\alpha = \alpha_0(1 + q_1\xi + q_2\xi^2 + q_3\xi^3 \ldots) \quad (9)$$

with the expansion constants q_i.

As follows from Eq. (8), the variable ξ (and consequently α) will depend on the spherical angles θ, φ, the incident spin current h_s, the applied magnetic field h, and the magnetization anisotropy H_k. To determine the expansion coefficients q_i, we made numerical estimations showing that the strongest influence on ξ is caused by the applied field h, which was assumed to be in the range $h=0$ to 30. The maximum values reached by ξ suggested the expansion coefficients $q_{1,2} \simeq 0.5$; higher-order terms in Eq. (9) were neglected. In this way, the contributions of the first two terms into the value of α appeared to be close to 10% and 2%, respectively, which agrees well with the expectation that in a Taylor expansion the influence of higher-order terms is progressively smaller.[48]

The characteristic angular distributions of the damping coefficient for different injected spin current h_s and applied

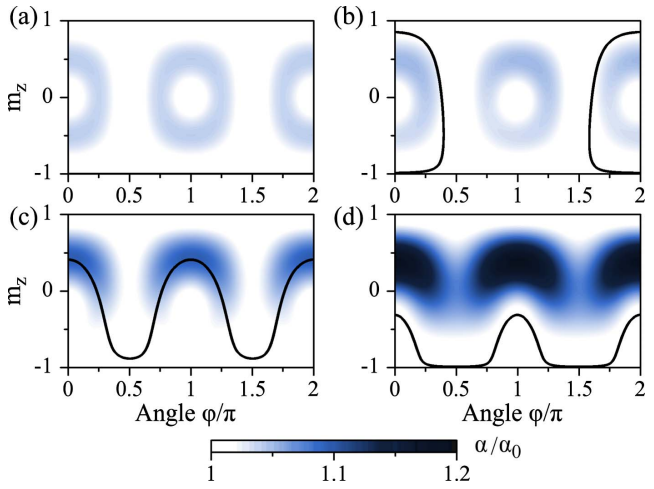

FIG. 1. (Color online) Angular dependence of the damping coefficient α for different values of spin current and applied magnetic field: (a) $h_s=h=0$; (b) $h_s=0.53$, $h=1.35$; (c) $h_s=0.27$, $h=6.65$; (d) $h_s=0.22$, $h=14$. The black curves represent the corresponding phase trajectories of the macrospin magnetization vector obtained for the initial value of $m_z^0 \approx -1$.

magnetic field h are shown in Fig. 1. As can be seen from this figure, the distribution of α is nonlinear and varies significantly with the applied field. Larger fields increase the rate of magnetic energy dissipation in certain areas of the plane $[m_z=\cos\theta,\varphi]$. In particular, for zero field and current, the distribution of α forms faint "rings" around the points $\varphi=0$, π and $\theta=\pi/2$ [Fig. 1(a)], where the values of the damping coefficient are slightly elevated ($\approx 1.05\times\alpha_0$), while outside them $\alpha=\alpha_0$. Hence, the phase trajectory describing the magnetization dynamics of the macrospin may not "feel" the damping changes if it does not enter into such areas [see OPP cycle, Fig. 1(b)] or on the contrary, can experience a higher energy dissipation rate in certain parts of the trajectory [see IPP cycle, Fig. 1(c)]. For larger applied fields, the damping variation becomes more significant, creating the whole "band" of high damping in the upper hemisphere [Fig. 1(d)]. Such a continuous area with higher dissipation level will make it more energetically beneficial for the phase trajectory to be located entirely in the areas of low damping.

It is worth mentioning that under the considered conditions the action of the high-dissipation "barrier" was not strong enough to keep the magnetization locked in the upper hemisphere even if one sets the initial orientation of the macrospin in the vicinity of the upper pole $m_z \approx +1$. Such locking would be beneficial due to the introduction of the narrow-angle in-plane precession cycle, attainable in the vast area of the $[h,h_s]$ phase diagram as reported in Ref. 47. However, to reproduce the latter results we needed to increase both q_1 and q_2 significantly so that the ratio α/α_0 will grow far beyond the acceptable range ($\approx 2\div 10$), jeopardizing the validity of the expansion (9).

To study the action of the alternating fields and currents, we have used four different types of pulses (Fig. 2) described by the following time dependencies:

$$Q^H(t) = Q\,\sin\left\{H\left(2\pi f_Q t-\frac{\pi}{2}\right)\left[2\pi f_Q t-\frac{\pi}{2}\right]+\frac{\pi}{2}\right\},$$

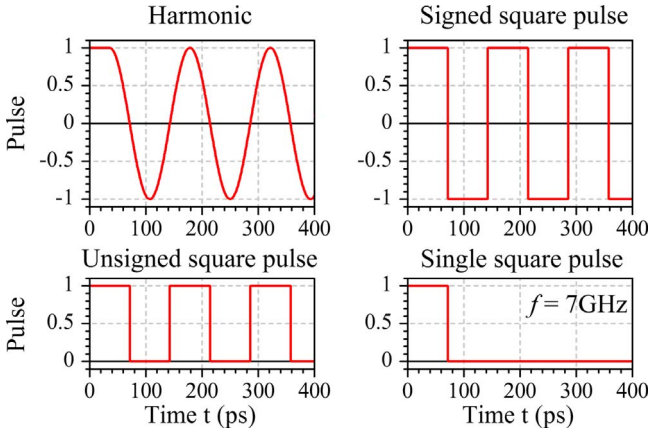

FIG. 2. (Color online) Time profile of the pulses used in the paper.

$$Q^S(t) = Q\ \mathrm{sgn}[\sin(2\pi f_Q t)],$$

$$Q^U(t) = \tfrac{1}{2}Q\{\mathrm{sgn}[\sin(2\pi f_Q t)]+1\},$$

$$Q^1(t) = QH(\pi-2\pi f_Q t), \tag{10}$$

where $Q=h,h_s$ and $H(x)$ is the Heaviside step function; the superscripts refer to the harmonic pulses (H), signed (S), unsigned (U) and single (1) square pulses. The time duration for the positive and negative parts of the pulses (when applicable) is equal allowing easy cross-comparisons of the results obtained. As we know, the macrospin approaches the stationary state in the absence of magnetic field and spin currents.[38] Therefore, the signal intended to excite the magnetic oscillations should not start with a reduced amplitude during the initial dozens of picoseconds, otherwise magnetization relaxation will take place and the macrospin will be locked in the ground state. For this reason, the first quarter period of the harmonic sine pulse was set to unity to ensure immediate action of the applied pulse. It is also worth mentioning that we will use the term "frequency" also for the case of a single pulse (where it is not in fact applicable in the strict sense due to the absence of periodic field/current oscillations). However, this approach allows us to simplify the further analysis. If required, the pulse duration can be easily obtained from the data presented in the figures as $t_{\mathrm{pulse}}=(2f_Q)^{-1}$.

Special attention should be paid to the proper selection of the frequencies f_h and f_{hs}. In particular, for $f_{h,hs} \ll \tau_0^{-1}$ the action of the external driving force is negligible because its variation is slow compared to the time scale of the magnetization precession. For $f_{h,hs} \approx \tau_0^{-1}$ the macrospin can track the applied pulses without reaching the steady precession / equilibrium state. Extremely high frequencies $f_{h,hs} \gg \tau_0^{-1}$ will make magnetization oscillations chaotic. Therefore, the synchronization with the external microwave can be achieved only when the driving force has a frequency larger than τ_0^{-1} and at the same time not overcoming the intrinsic frequency of the stable magnetization precession, that is, about 30 GHz. Our previous studies[49] revealed that the maximum amplitude of steady magnetization precession observable under the

magnetic fields and current polarization vectors collinear with the easy magnetization axis of an analyzer layer with the parameters of Co is about 7 GHz. Therefore this frequency and the doubled frequency (14 GHz) were investigated in this paper as the most possible candidates to trigger large-amplitude magnetization oscillations. It is also worth special attention that the time-dependent h and h_s will automatically cause the temporal variations of the damping coefficient α according to Eqs. (8) and (9), making the "damping landscape" (Fig. 1) time varying following the oscillating driving force.

III. EFFECT OF AN ALTERNATING CURRENT ON THE MACROSPIN DYNAMICS

To simplify the analysis of the magnetization dynamics excited by alternating spin-polarized currents and magnetic fields, we would like to present a brief illustration of the macrospin behavior under constant h_s and h. One of the most useful and direct ways to visualize the boundaries between different dynamic modes of the system in the space of control parameters involves the use of a dynamic phase diagram.[49,50] Aiming to separate a simple magnetic moment reversal from its periodic oscillation and chaotic motion for the case when the synchronization with the incident microwave is absent, we calculate the Hausdorff dimension defined as[51]

$$D_H = \lim_{\epsilon \to 0} \frac{\log N}{\log \epsilon^{-1}}, \tag{11}$$

where N is the number of n-dimensional cubes with side ϵ covering the phase trajectory. If the system converges to a single state resulting in a pointlike phase portrait, the Hausdorff dimension is zero. For the case of chaotic oscillations covering the whole phase sphere, the dimension tends to the value $D_H=2$. For periodic oscillations of the moment, when the phase portrait represents a limit cycle, its dimension is $1 \leq D_H \leq 2$. The inclusion of additional loops to the phase trajectory increases the spatial density of the phase portrait, and the resulting dimension D_H is larger. At the same time, the variation of the precession speed without a modification of the phase portrait does not introduce any significant changes to D_H.

Figure 3 presents a diagram of the Hausdorff dimension $D_H(h,h_s)$ discerning the main oscillatory modes—in-plane precession [dark blue (online) / gray (print) area, Fig. 3(a)] and out-of-plane precession [light blue / gray area, Fig. 3(b)]. The characteristic time dynamics of the individual magnetization vector projection and the corresponding Fourier spectra are shown at the bottom of this figure. As one can see, in the IPP case the component m_x performs symmetric sign-changing oscillations, so that observing the system for a long time one gets the impression that $\bar{m}_x=0$, as if all the magnetization dynamics takes place in the easy magnetization plane. The OPP phase portrait is characterized by a single sign of m_x, shifting the time-averaged dynamics out of the easy plane. It is important to emphasize that the oscillations of the m_z component (measurable in GMR) in both cases are practically equal, rendering the same oscillation frequency of

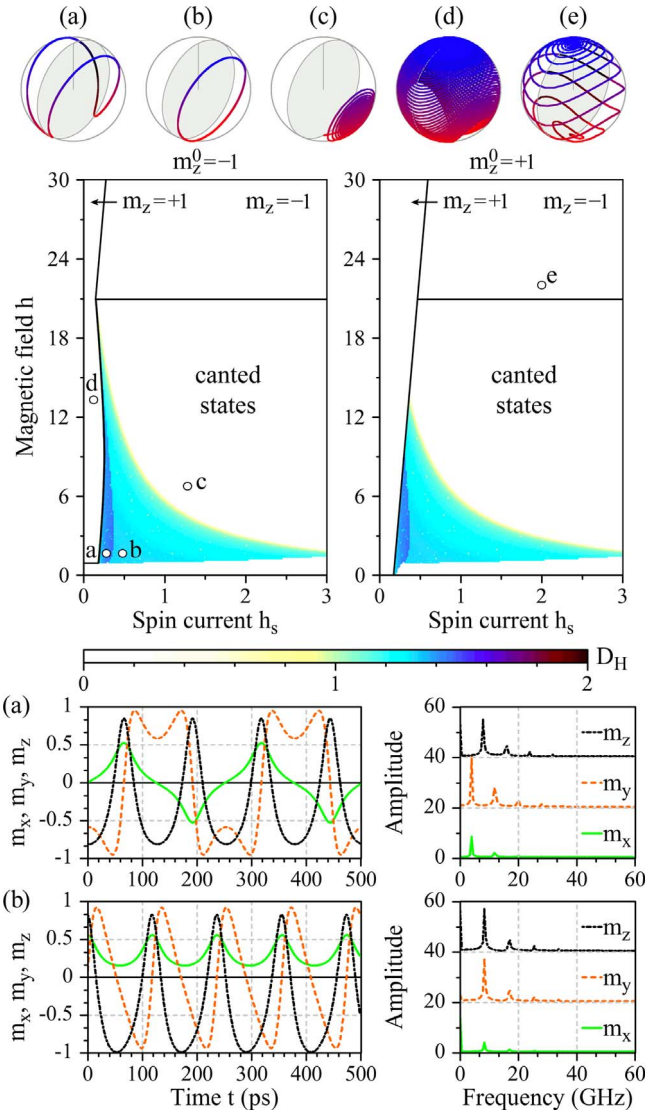

FIG. 3. (Color online) Hausdorff dimension phase diagram of the system for time-independent h and h_s. The panels present the data calculated for the initial magnetization $m_z^0=-1$ (left) and $m_z^0=+1$ (right). The most characteristic phase portraits are the following: (a) in-plane precession cycle ($h_s=0.28$, $h=1.65$); (b) out-of-plane precession cycle ($h_s=0.48$, $h=1.65$); (c) magnetization precession to reach a canted state ($h_s=1.28$, $h=6.75$); (d) slow precessional magnetization reversal from $m_z^0=-1$ to $m_z=+1$ ($h_s=0.12$, $h=13.3$); (e) faster switching from $m_z^0=+1$ to $m_z=-1$ ($h_s=2$, $h=22$).

7 GHz. However, due to two times longer projection of the phase trajectory on the m_x,m_y plane in the case of the IPP cycle, the main spectral peaks for m_x and m_y have halved frequency.

White areas in Fig. 3 correspond to $D_H=0$, i.e., when the system converges either to the upper (lower) pole of the unitary sphere or relaxes to a canted state via slow magnetization precession [Fig. 3(c)]. The reorientation rate of the magnetization vector depends on the attraction force of the corresponding stationary state. Thus, the magnetization reversal from $m_z^0 \approx -1$ to $m_z=1$ [Fig. 3(d)] under the given combination of h and h_s can be characterized by slow coiling

of the phase trajectory out of an unstable IPP cycle to a faintly attracting upper pole, taking about 2300 ps to reach the pole. The switching time τ_{sw} was determined as the period required for the phase point to get to $\theta \geq 0.99\pi$ or $\theta \leq 0.01\pi$ from the initial state $m_z^0 \approx +1$ and $m_z^0 \approx -1$, respectively. To overcome the numerical issues connected with abrupt thresholding, the time distribution of m_z was smoothed within a window of 100 ps. The calculated values of the Hausdorff dimension were used to determine the applicability of the switching time notion, which can be used only when the final magnetization state is fixed ($D_H=0$). The magnetization reversal from the state $m_z^0 \approx +1$ to $m_z=-1$, illustrated in Fig. 3(e), runs faster due to a larger attraction force of the lower pole, yielding the switching time $\tau_{sw}=500$ ps. The two initial macrospin orientations m_z^0, shown in the left and right panels of Fig. 3, reveal the hysteretic effect, shifting the line corresponding to the boundary between the states $m_z=+1$ and $m_z=-1$ toward higher currents.

Small initial deviations from the stationary state for a macrospin subjected to a sign-alternating spin current, either in the form of harmonic (h_s^H) or square signed pulses (h_s^S), appear to be effectively suppressed, locking the system in the corresponding pole. However the unsigned square current pulses (h_s^U) creating an interrupting current signal can drive the system into oscillatory states and cause the magnetization reversal. Though, as the influence of the current is not continuous, the dynamical diagram of the system is anticipated to become noisy. Most stable phase portraits can be obtained in the case of longer current pulses and, therefore, for smaller frequencies f_{hs}.

A. Square unsigned current pulses

A characteristic example of the phase diagrams for $f_{hs}=7$ GHz is shown in Fig. 4. As we see, this phase diagram is roughly similar to the dc case illustrated in Fig. 3. The main difference consists in the shift of the area corresponding to the reversal between $m_z=+1$ and $m_z=-1$ toward larger spin currents. This behavior is predictable because the interruptive current will be required to have a larger magnitude to render a torque comparable to that supplied by a constant current. In general, all the areas corresponding to IPP, OPP, and canted states become blurred and noisy. As the spin current is injected in pulses and is equal to zero otherwise, the synchronization with $h_s(\tau)$ may cause the coupling of the oscillation modes, i.e., the system may exhibit IPP oscillations when the pulse is on and OPP oscillations when it is off [Fig. 4(a)], or jump between the different OPP trajectories [Fig. 4(e)]. Note that for the former case the time profiles and the Fourier spectra of individual magnetization components shown at the bottom also display the superposition of IPP and OPP features for the m_y and m_z components, clearly notable under comparison with the corresponding data presented in Figs. 3(a) and 3(b). Lower magnetic fields in combination with larger currents make the precession cycles noisy [Fig. 4(b)]. At the high-field boundary limiting the region of canted states one can see a narrow wedge-shaped area corresponding to small-amplitude ($\Delta m_z \approx 0.18$) in-plane precession [Fig. 4(c)], also becoming noisy with increasing current.

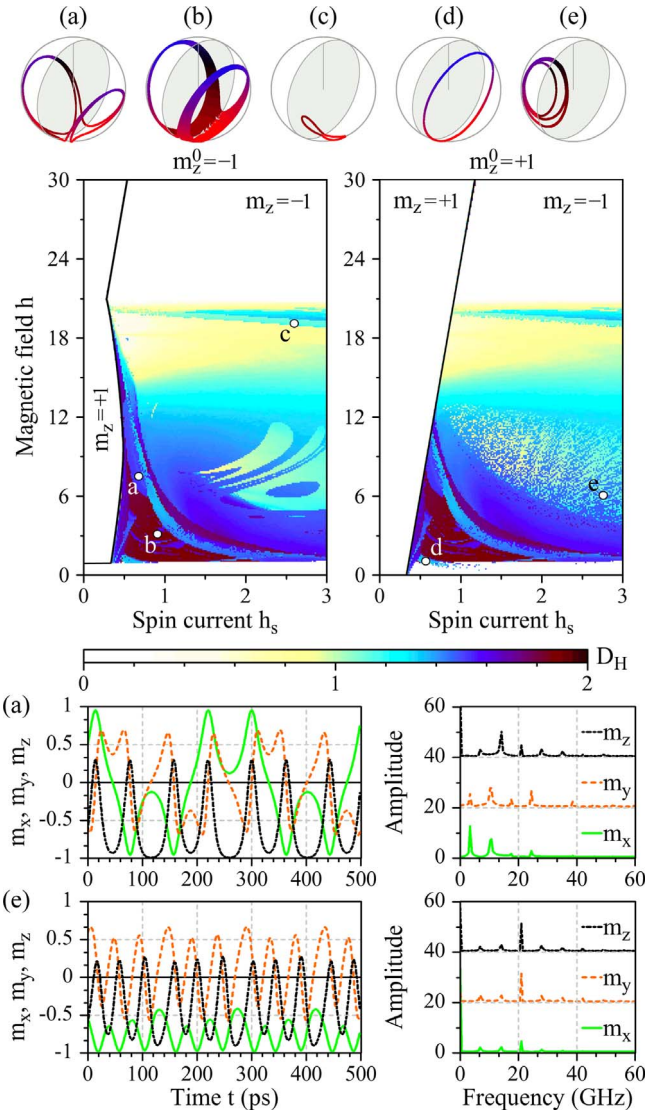

FIG. 4. (Color online) Macrospin dynamics under time-alternating spin current ($f_{hs}=7$ GHz) with square unsigned peaks. The darker areas correspond to lower synchronization level. The panels present the data calculated for the initial magnetization $m_z^0=-1$ (left) and $m_z^0=1$ (right). The most characteristic phase portraits are the following: (a) mixture of in-plane and out-of-plane precession cycles ($h_s=0.68$, $h=7.5$); (b) noisy IPP cycle ($h_s=0.91$, $h=3.1$); (c) small-amplitude IPP ($h_s=2.6$, $h=19.1$); (d, e) OPP cycles ($h_s=0.57$, $h=1.05$ and $h_s=2.76$, $h=6.05$, respectively).

For initial macrospin orientation in the vicinity of the upper pole $m_z^0 \approx +1$ (Fig. 4, right panel), large-amplitude OPP cycles [Fig. 4(d)] can be obtained also under magnetic fields $h<1$, which is smaller than the limit $h_{\text{lower}}=1$ for the constant spin current.[38] These oscillation modes, excitable at a minimal field, can be important for device applications. Moreover, the wide region on the h, h_s plane corresponding to the canted states in a constant injected current h_s becomes partially populated with the states characterized by three-loop OPP cycles with oscillation frequency $3f_{hs}$ [Fig. 4(e) and the corresponding bottom panel]. Therefore, under the pulsed spin current, the macrospin exhibits a wider variety of oscillation modes, including those achievable at lower fields

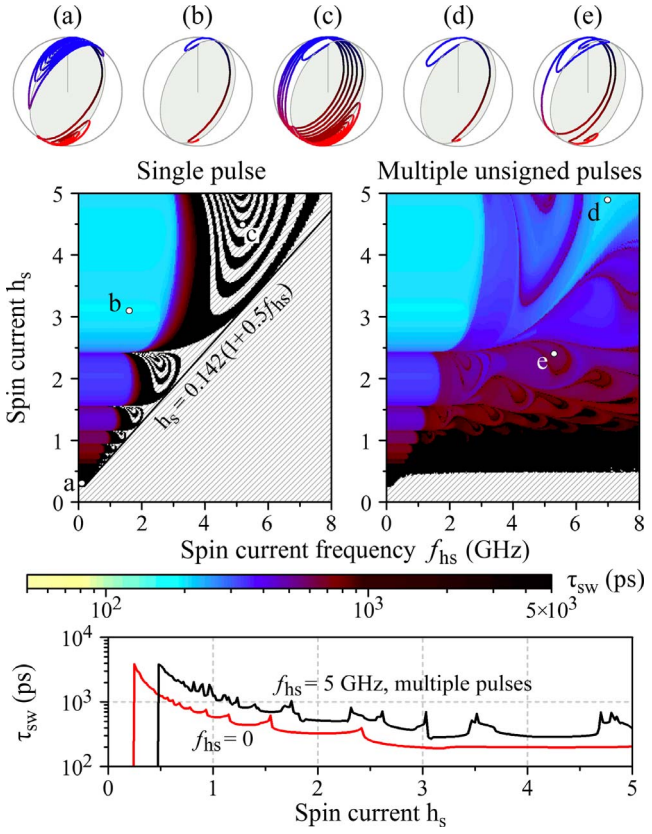

FIG. 5. (Color online) Macrospin reversal under the action of a single spin current pulse (left panel) or multiple pulses (right panel) with the amplitude h_s and frequency f_{hs}; magnetic field is absent (h=0). The most characteristic switching trajectories are shown for the following: (a) f_{hs}=0.1, h_s=0.3; (b) f_{hs}=1.6, h_s=3.1; (c) f_{hs}=5.2, h_s=4.5; (d) f_{hs}=7, h_s=4.9; (e) f_{hs}=5.3, h_s=2.4. The line plotted in the left panel defines the limit h_s/f_{hs} ratio, below which the pulse amplitude is weak enough to perform macrospin magnetization reversal. The lower panel shows the current profiles (vertical sections) of the plots at f_{hs}=0 and f_{hs}=5 GHz for the case of the current injected in multiple pulses.

or in wide areas corresponding to a fixed magnetization vector under direct current injection, offering promising opportunities for devices performing transformation of rectangular current signal into high-frequency harmonic magnetization oscillations.

B. Macrospin reversal by a single current pulse

Experimental research confirms that even a single current pulse can be used for efficient magnetization switching.[22] We calculated the dependence of the switching time τ_{sw} on the pulse frequency f_{hs} and amplitude h_s for the case of single and multiple current pulses with square unsigned profile (see Fig. 5, left and right panel, respectively). The initial macrospin orientation was set to $m_z^0 = +1$. The combinations of the control parameters that do not yield magnetization reversal are represented with a diagonally-dashed area. As one can see, the magnetization reversal by a single pulse is possible only for the currents surpassing h_s=0.25 at the frequencies $f_{hs} \ll 1$, which corresponds to the case of a dc current. (See the dynamic diagram presented at the right panel of Fig. 3.) However, the switching time τ_{sw} for a low-current reversal is large (2500 ps) due to the excessive magnetization ringing around the bottom and upper poles in the vicinity of the easy magnetization plane [Fig. 5(a)]. The single-pulse reversal appears to be possible roughly in a triangular-shaped area that can be fitted by the expression

$$h_s \geq 0.142(1 + 0.5 f_{hs}). \tag{12}$$

That is, for shorter pulses (larger f_{hs}) higher injected currents will be required to trigger magnetization reversal. For the case f_{hs}=0 (dc current) the switching time $\tau_{sw}(h_s)$ (Fig. 5, bottom panel) features a distinct quantization effect,[52] which holds for higher frequencies if the magnitude of the injected current is large enough, so that the time period required to achieve switching between the opposite macrospin orientations is constant over a certain range of f_{hs}, reducing the need for precise fine tuning of current pulse duration. The lowest switching time τ_{sw}=193 ps was registered for the phase portrait approaching BMR [Fig. 5(b)]; this switching time is attainable for a single current pulse with duration of 170 ps and above. For current pulse frequencies slightly lower than those obtained from condition (12), the attraction basins of upper and lower pole become intermixed in the $[f_{hs}, h_s]$ plane [similarly to the results obtained by Sun and Wang (Ref. 53)], so that the slight changes in the amplitude or duration of the current pulse may succeed or fail to perform the macrospin switching. Even if the latter takes place, the corresponding phase trajectory becomes much complicated by numerous precession loops resembling out-of-plane cycles [Fig. 5(c)], increasing the switching time to nanoseconds.

Application of multiple current pulses introduces significant changes for the case when one pulse was not enough to perform the (fastest) switching (Fig. 5, right panel), introducing the wide switching area to the right of the division line [Eq. (12)]. At small currents ($h_s < 1$), the magnetization switching time is over 1000 ps due to significant ringing. For $f_{hs} > 6$ GHz one can achieve the switching time 200 ps [Fig. 5(d)]. Introduction of the additional precession cycles increases the reversal times to 600 ps [Fig. 5(e)] and above. It is also important to emphasize that the current dependence of the switching time calculated for higher current frequencies [e.g., f_{hs}=5 GHz (pulse length 100 ps), see Fig. 5, bottom panel] also features reversal time quantization, which, however, is less pronounced and allows either an increase or decrease in the switching time, on the contrary to the stable decrease observed for the dc case.

Thus, the macrospin described by the parameters of Co can have the magnetization reversal time on the order of 200 ps without any optimization of the temporal pulse profile[26] and avoiding the necessity of finding a special angle for the application of a spin current pulse relative to the easy magnetization axis.[20,23,34]

The crucial role in gaining the required reversal time appears to belong to the proper pulse amplitude adjustment. The application of multiple pulses allows to achieve switching for larger frequencies, but the corresponding τ_{sw} is at least two times higher.

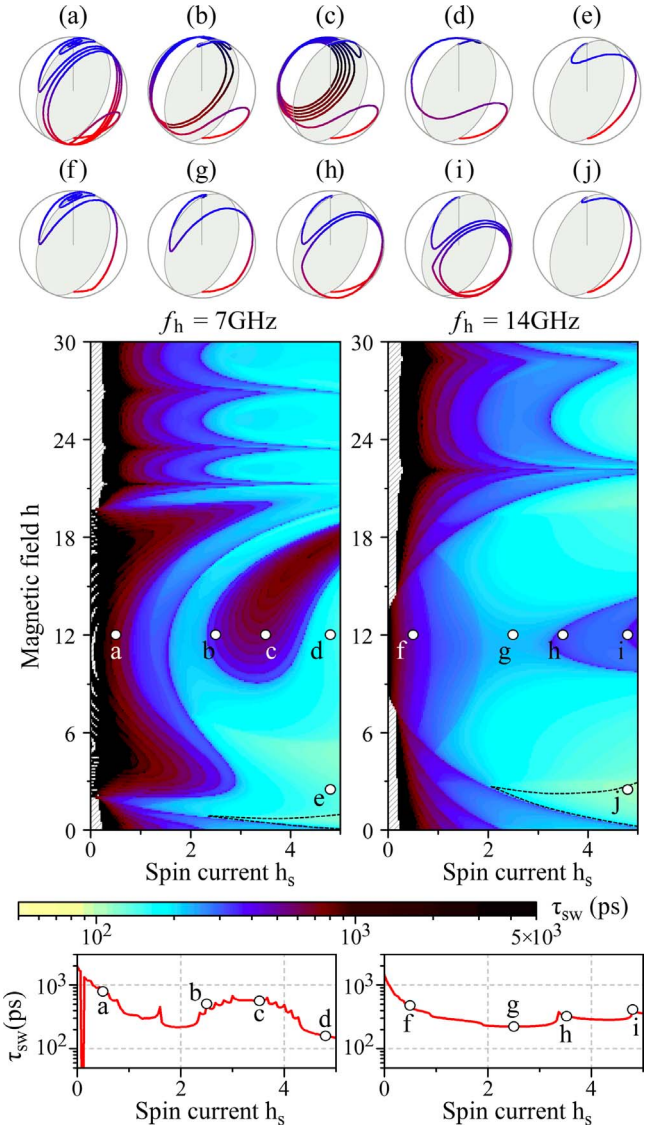

FIG. 6. (Color online) Magnetization switching assisted by a single pulse of magnetic field corresponding to the frequencies f_h =7 GHz→t_{pulse}=71.43 ps (left panel) and f_h=14 GHz→t_{pulse} =35.71 ps (right panel) as a function of h and h_s. The dashed-line contour denotes the ballistic magnetization reversal area. The bottom panel shows the dependence of the switching time $\tau_{sw}(h_s)$ for h=12. The most characteristic phase portraits are the following: for h=12—(a,f) h_s=0.5, (b,g) h_s=2.5, (c,h) h_s=3.5, (d,i) h_s=4.8; for h=2.5—(e,j) h_s=4.8.

IV. INFLUENCE OF VARIABLE MAGNETIC FIELDS ON THE MACROSPIN DYNAMICS

A. Macrospin reversal assisted by a field pulse

Magnetization reversal can be also achieved by applying the rectangular pulses of the magnetic field to a macrospin, subjected to a dc spin current. The results of corresponding simulations for the case of single pulse are illustrated in Fig. 6 for two frequencies: f_h=7 GHz (left panel) and f_h =14 GHz (right panel). As we see, the dependence of the switching time on h,h_s and f_h is significantly nonlinear and complicated. The typical cross sections of two-dimensional plots for the constant field h=12 are presented in the bottom panel of the figure, showing pronounced quantization of τ_{sw} with increasing reversal time for each new ringing loop that appears. For lower field frequency the switching times are higher, forming a wide maximum roughly centered around $h_s \approx 3.2$ for h=12. High switching times exceeding half-nanosecond are caused by formation of the OPP loops [Figs. 6(a)–6(c)]. The fastest switching attained runs for about 150 ps [Fig. 6(d)] and 140 ps [Fig. 6(e)].

For a higher field oscillation frequency, the magnetization ringing may appear either close to the upper pole [Fig. 6(f), τ_{sw}=450 ps] or in the vicinity of out-of-plane precession trajectory [Fig. 6(h), τ_{sw}=320 ps; Fig. 6(i), τ_{sw}=390 ps]. Similarly to the low-frequency mode, magnetization reversal almost devoid of the ringing is attainable for the spin currents between these groups of points [Fig. 6(g), τ_{sw} =220 ps]. It is extremely important to emphasize that magnetization switching along the ballistic trajectory [e.g., Figure 6(j), τ_{sw}=110 ps] is achievable in a wedge-shaped area in the parameter space [h,h_s], denoted with a dashed-line contour in the figure for $h_s > 2$ and $0 < h < 3$. This BMR area is present in all further $\tau_{sw}(h,h_s)$ plots, featuring significant shape variation depending on the time profile and frequency of the pulses. The switching time achievable for the phase portraits belonging to the BMR area is about 100–200 ps, which is in good agreement with the experimental value of 165 ps reported for the ultrafast magnetization switching by Schumacher *et al.*[28] Despite other areas in calculated τ_{sw} plots may also exhibit magnetization reversal with a similar rate; their phase portraits feature significant deviation of the magnetization trajectory from the easy plane [Figs. 6(d) and 6(e)], or possess a complicated topology with several loops or extensive ringing around the target pole. Moreover, such fast-switching areas are usually situated at much higher field values, requiring approximately ten times larger h than that necessary for the BMR.

Therefore, our numerical simulations revealed the presence of a limited area of parameter values located at low fields, where the magnetization reversal takes place in the closest vicinity of the easy magnetization plane and the total reversal times are similar to the experimentally observed values approaching the ultrafast switching limit.[28] This finding, in our opinion, is of the utmost importance both for fundamental and applied points of view, allowing to predict the optimal set of control parameters required to achieve macrospin magnetization switching along the shortest trajectory possible.

In contrast to the previously discussed effect of the sign-variable spin currents locking the system in the equilibrium state, the application of h^H, h^S and h^U field pulses can switch the moment to one of the precessional states due to synchronization with the periodic driving force. To determine possible cases when such a synchronization is attainable, we consider a multidimensional optimization task in the space of [h, h_s, f_h] with an additional freedom degree describing the pulse type. Here we present the most representative two-dimensional dynamic diagrams in the [h,h_s] space, constructed for the case when two other parameters are constant.

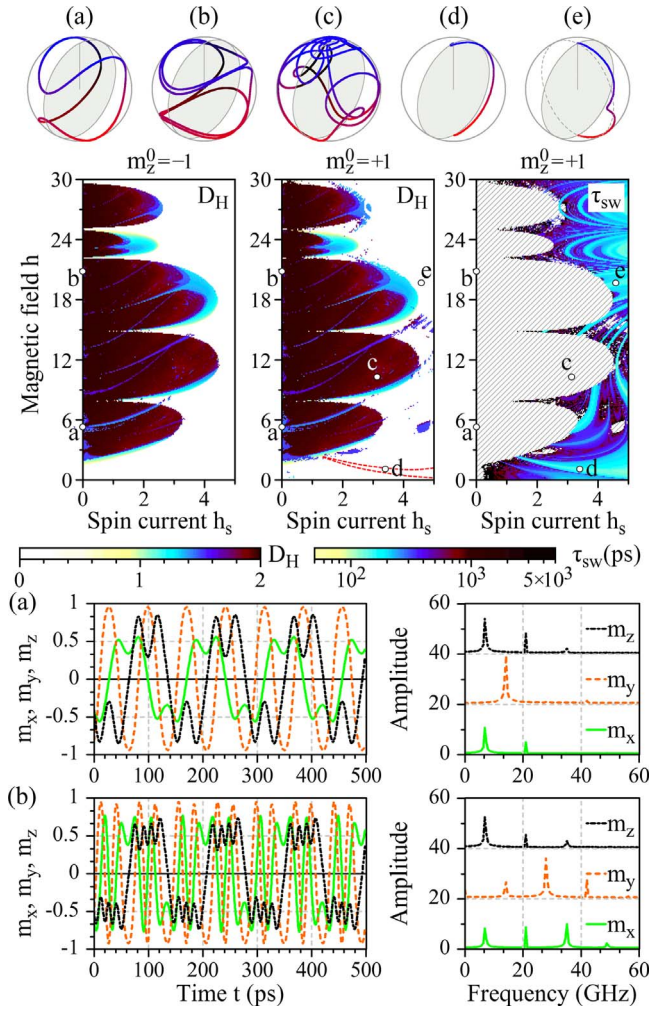

FIG. 7. (Color online) Synchronization diagram for a macrospin subject to the harmonic magnetic-field oscillations with the frequency f_h=7 GHz. The white areas correspond to the parameter combination when the resulting magnetic moment remains in the equilibrium; dark areas correspond to the absence of the synchronization. The dashed-line contour in the central panel denotes the ballistic magnetization reversal area. The rightmost panel presents the switching time dependence $\tau_{sw}(h_s,h)$; if switching time notion is inapplicable, the corresponding areas are diagonally dashed. The most characteristic phase portraits are the following: (a) h_s=0, h =5.3; (b) h_s=0, h=20.85; (c) h_s=3.13, h=10.3; (d) h_s=3.4, h=1.1; (e) h_s=4.58, h=19.7. For the last phase portrait, the contour perpendicular to the easy magnetization plane is supplied as a guide to the eyes.

B. Harmonic field pulses

Figure 7 displays the dynamic diagram for the system subject to a harmonically modulated magnetic field h^H with the frequency of f_h=7 GHz. As we see, for both initial values of $m_z^0 \approx \pm 1$, there are large regions in the parameter space, for which the synchronization is absent and the magnetization vector cannot attain any periodic motion, covering the unitary sphere with chaotic trajectory, so that $D_H \approx 2$ (dark areas in Fig. 7). For large spin currents, the pulsing field is unable to move the magnetization out of the equilibrium state, resulting in $D_H \to 0$ (white areas in Fig. 7). In the absence of injected current, the macrospin synchronizes to the external driving force within several field intervals, the largest of which is located at $h<6$. The resulting phase portraits represent the variations of IPP precession with a number of loops increasing together with the applied field [Figs. 7(a) and 7(b)]. As one can see from the temporal profiles of magnetization components, an increase in the loop number leads to formation of high-frequency oscillation "packets" in $m_z(t)$, which can be observed experimentally in GMR measurements. As the amplitude of these oscillations is smaller than that of the main signal, they correspond to secondary peaks in the fast Fourier transform (FFT) spectra with the frequencies surpassing the exciting wave frequency several times. The formation of such high-frequency packets can be important for applications because it allows designing a device of variable resistivity, much faster as compared to the variation of the driving magnetic signal. It is also important to emphasize that for $h_s \neq 0$, in the parameter-space area where the synchronization is usually absent, one observes narrow bands or islands of synchronized motion, leading to complex magnetization oscillations as presented in Fig. 7(c). Upon changing the initial orientation of the macrospin from $m_z^0=-1$ to $m_z^0=+1$, the synchronization plots become slightly modified due to the hysteresis effects, which take place at larger applied currents $h_s \gtrsim 2$ (Fig. 7, central panel). The switching time diagram (Fig. 7, rightmost panel) was obtained for the initial upward macrospin orientation, calculating the time required to reach the vicinity of $m_z=-1$ by applying the technique described in Sec. III. As we see, the dependence of the switching time on the control parameters h and h_s is significantly more nonlinear than that obtained under single square pulses (Fig. 6). Ballistic magnetization reversal is attained in quite a wide area under the fields h <2, with the phase trajectory almost tracing the meridian lying in the easy magnetization plane [Fig. 7(d), τ_{sw} =140 ps]. Surprisingly, the application of high fields and currents allows to perform fast switching even along the trajectory almost following a meridian *perpendicular* to the easy magnetization plane [Fig. 7(e), τ_{sw}=145 ps].

In the case of harmonic field oscillations with frequency f_h=14 GHz, the synchronization areas are growing in size, and the hysteresis effects under the flip of m_z^0 are more pronounced. It is worth mentioning that the use of high-frequency harmonic oscillations of the field enables to obtain the steady precession for $h_s \to 0$ and $h \ll 1$. For small spin currents, the islands of synchronized motion $D_H \approx 1$ expand significantly, allowing to get a large-amplitude out-of plane precession cycle [Fig. 8(a)] with the frequency corresponding to that of the driving force. Upon approaching the boundary of the synchronization island, the precession trajectory becomes more complex [Fig. 8(b)]. A hybrid phase trajectory possessing two OPP cycles and a small-amplitude IPP cycle [Fig. 8(c)] can be attained in the synchronization island of considerable size located at the fields of h=12.5 to 16. More complicated forms are also available [Fig. 8(d)] in some small synchronization windows, the size of which seems to preclude the practical use of these modes due to the difficult adjustment of control parameters.

The switching time diagram shown in the rightmost panel of Fig. 8 is more complicated than the similar one obtained

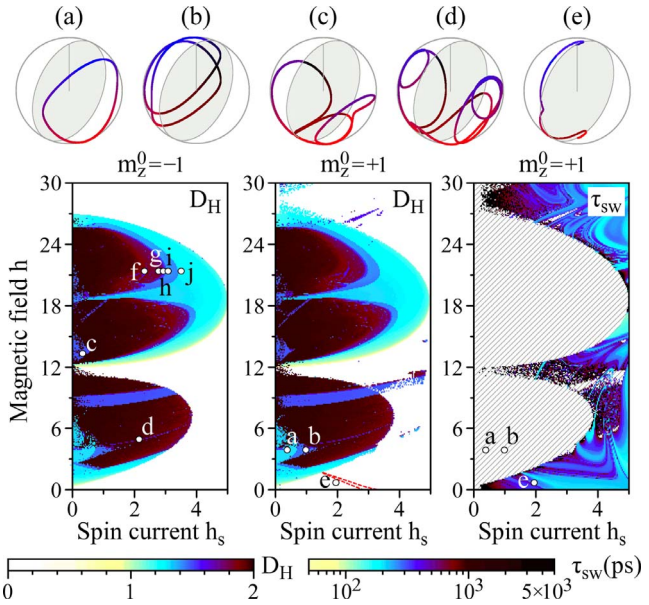

FIG. 8. (Color online) Macrospin synchronization diagram under harmonic magnetic-field oscillations with f_h=14 GHz. The most characteristic phase portraits are the following: (a) h_s=0.38, h=3.9; (b) h_s=0.98, h=3.9; (c) h_s=0.33, h=13.5; (d) h_s=2.15, h=4.95; (e) h_s=1.95, h=0.7. The phase portraits for the points (g–j) are shown in Fig. 9. The dashed-line contour in the central panel denotes the BMR area.

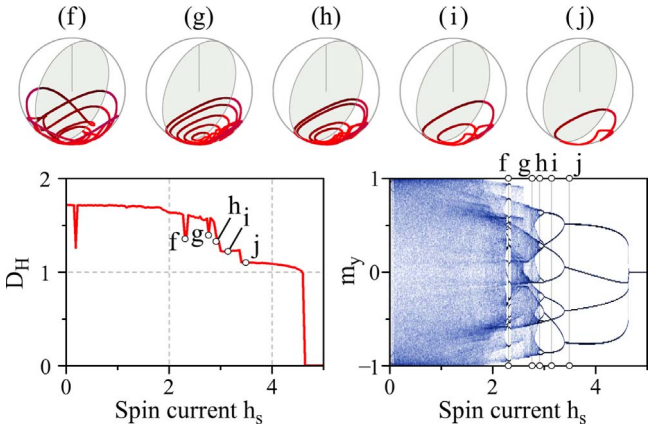

FIG. 9. (Color online) Hausdorff dimension (left panel) and the bifurcation diagram (right panel) showing period halving bifurcation cascade for the macrospin under oscillating magnetic field h =21.4, f_h=14 GHz. The most characteristic phase portraits are the following: (f) h=2.32; (g) h=2.77; (h) h=2.93; (i) h=3.08; (j) h =3.5.

for half field frequency (see Fig. 7). As one can see from the figure, the BMR area for f_h=14 GHz becomes narrower due to the increased precision demand for the corresponding pairs of h and h_s values due to shorter field pulses. The reversal times attainable in this case are on the order of 200 ps. An interesting switching mode with a two-segment trajectory similar to that shown in Fig. 7(e) but situated roughly in the easy magnetization plane could be observed in the close vicinity of the BMR area [Fig. 8(e), τ_{sw}=250 ps].

Another important feature revealed by the calculations is the characteristic period halving bifurcation cascade[51] observable under the spin current variation [Figs. 8(g)–8(j)]. Figure 9 presents a profile of the Hausdorff dimension and the bifurcation diagram for the m_y component (left and right panels, respectively). The bifurcation diagram was obtained according to the standard procedure,[51] plotting the points corresponding to the local maxima and minima of the $m_y(\tau)$ dependence at a fixed h_s. The period halving bifurcations are clearly discernible by the decrease in the number of loops composing the phase portrait, pronounced horizontal plateaus on D_H curve, and joining of bifurcation diagram branches [Figs. 9(g)–9(j)]. Taking into account the values of the spin current at the bifurcation points, we were able to show that the bifurcation cascade to the left of h_s=3.387 follows the Feigenbaum constant δ=4.6692016… (Ref. 51). For $0.01<h_s<2.3$ the system is chaotic, featuring small windows of synchronized motion [Fig. 9(f)]. Therefore, proper adjustment of the harmonically oscillating field allows driving the macrospin through the set of period halving bifurcations by tuning the spin current at a fixed field amplitude, resulting in corresponding steplike variations of the oscillation frequency that may have good application perspectives. The similar bifurcation cascades were also recently reported[54] in the macrospin simulations of the permalloy particles.

C. Sign-varying square field pulses

By applying the sign-alternating rectangular pulses of magnetic field, one observes that the dynamical response of the macrospin (Figs. 10 and 11) remains somewhat similar to the case of the harmonic driving force. The key difference

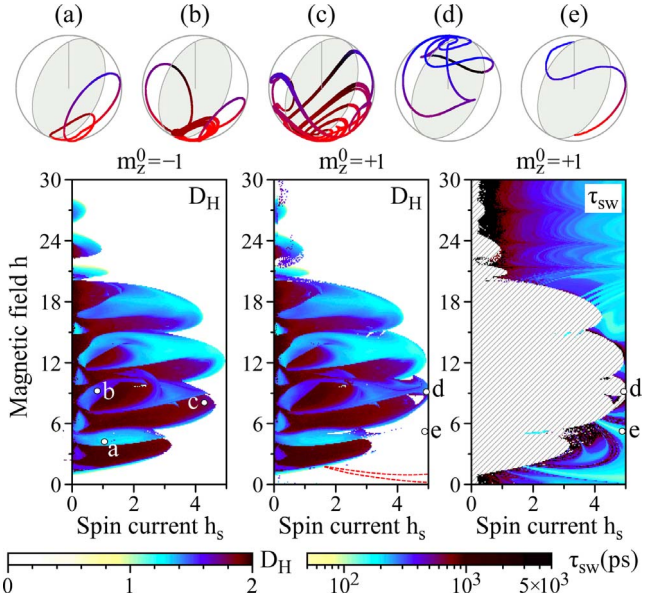

FIG. 10. (Color online) Macrospin synchronization with the sign-varying square-shaped field pulses with frequency f_h=7 GHz. The most characteristic phase portraits are the following: (a) h_s =1.05, h=4.2; (b) h_s=0.82, h=9.2; (c) h_s=4.28, h=8.05; (d) h_s =4.93, h=9.15; (e) h_s=4.88, h=5.25. The dashed-line contour in the central panel denotes the BMR area.

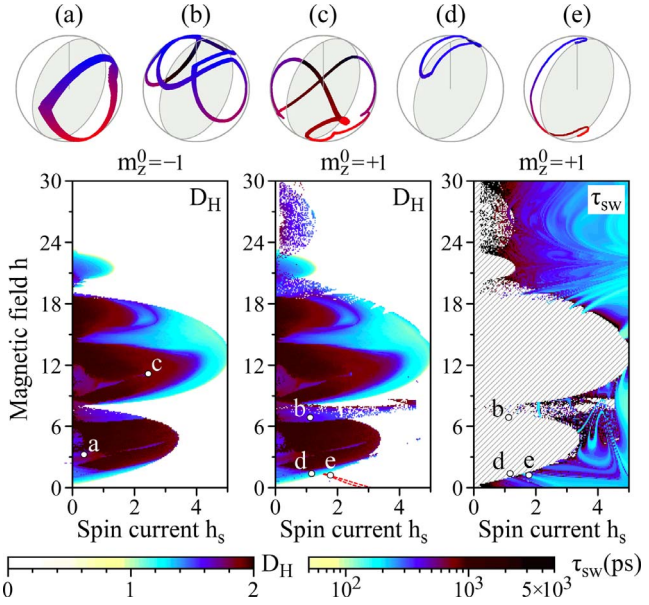

FIG. 11. (Color online) Synchronization diagram for a macrospin subject to square-shaped sign-alternating field pulses with the frequency f_h=14 GHz. Characteristic phase portraits are the following: (a) h_s=0.38, h=3.25; (b) h_s=1.12, h=6.9; (c) h_s=2.45, h=11.15; (d) h_s=1.17, h=1.4; (e) h_s=1.77, h=1.4. The dashed-line contour in the central panel denotes the BMR area.

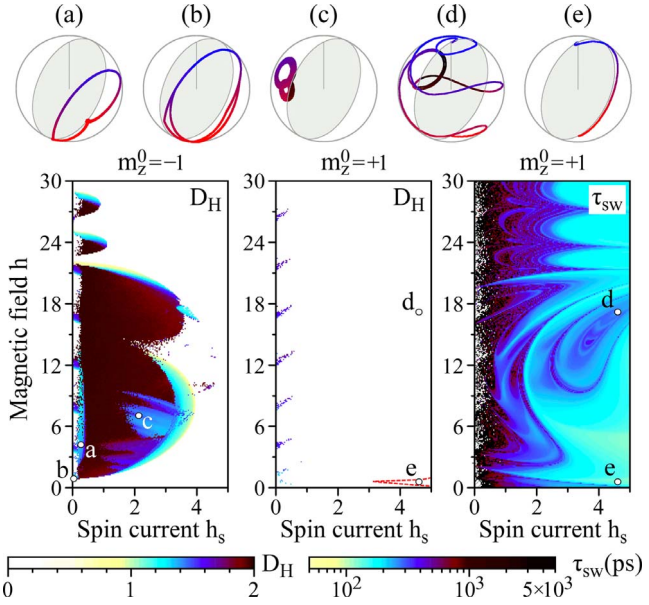

FIG. 12. (Color online) Synchronization diagram for the macrospin subject to the unsigned square-shaped microwave with the frequency f_h=7 GHz. Characteristic phase portraits are the following: (a) h_s=0.27, h=4.2; (b) h_s=0.04, h=0.9; (c) h_s=2.13, h=7.05; (d) h_s=4.6, h=17.2; (e) h_s=4.6, h=0.6. The dashed-line contour in the central panel denotes the BMR area.

concerns smaller field intervals, for which the applied signal can force the magnetization vector off the equilibrium state. In general, the areas of successful synchronization between the macrospin and the incoming microwave are significantly larger as compared to the h^H pulses, although the resulting phase portraits appear noisier due to the step-function nature of the pulses. Such a rough control method permits to form asymmetric phase portraits [see Fig. 10(a)], or generate magnetic oscillations with multiple loops, otherwise similar to the "clean" phase portraits reachable with the harmonic field pulses [e.g., compare Fig. 10(b) to Fig. 8(c) and Fig. 10(c) to Fig. 9(f)]. The hysteresis effects are less pronounced when h^S pulses are applied, but nevertheless allow to obtain a periodic magnetization motion [Fig. 10(d)] with no counterparts at the same current value in the left panel of Fig. 10. Contrary to the harmonic field oscillations, the square pulses result in a smoother switching time τ_{sw} landscape (compare the rightmost panel for Fig. 10 with Fig. 7 and Fig. 11 with Fig. 8), featuring a somewhat larger BMR area with a switching time of about 140–150 ps. However, a slightly faster magnetization reversal was observed for the trajectory significantly deviating from the easy plane [Fig. 10(e), τ_{sw}=110 ps].

For the magnetic-field pulses of frequency f_h=14 GHz, the phase portraits become noisier, as the time between successive pulses gets smaller, augmenting the influence of the macrospin orientation at the field reversal moment on the further dynamics of the system. Under these conditions, our numerical simulations yielded deformed and noisy versions of the OPP cycle [compare Figs. 11(a) and 8(a)] and a complex cycle with three loops [Fig. 11(b) vs Fig. 8(c)]. Poor synchronization can also result in nonsymmetric oscillations [Fig. 11(c)] which have low chances to be useful for device applications. In weak magnetic fields, the system is characterized by a narrow-angle precession around the easy magnetization axis [Fig. 11(d)]. The distribution of switching times as a function of h and h_s is reminiscent of that presented in Fig. 8 for the harmonic oscillations, although the BMR area appears to be slightly narrower. The switching trajectory has some minor ringing at both poles [Fig. 11(e)] and $\tau_{sw} \approx 200$ ps.

Therefore, the use of signed square field pulses results in positive widening of the synchronization region, but the obtained oscillation modes appear to be blurred for higher field frequencies, which makes them less attractive for applications than the modes attainable under a harmonic signal. However, the situation concerning magnetization switching is more favorable for abruptly changing h^S pulses, featuring smoother reversal time landscape (i.e., lowering the requirements for the precise tuning of h and h_s to obtain the desired τ_{sw}).

D. Unsigned square field pulses

The application of magnetic fields in the form of unsigned square pulses h^U changes the behavior of the system significantly (see Figs. 12 and 13). As the field is "pushing" the magnetization only in one direction and disappears for a certain period of time, it suppresses the initial deviations for the positive m_z^0, making almost all the $[h,h_s]$ parameter plane devoid of the areas with $D_H > 0$ (Fig. 12, middle panel). For large f_h the field pulses are shorter and follow each other faster, becoming more efficient in driving the macrospin out of the equilibrium, thus leading to an increase in the synchronization islands in the middle panel of Fig. 13. On-off field

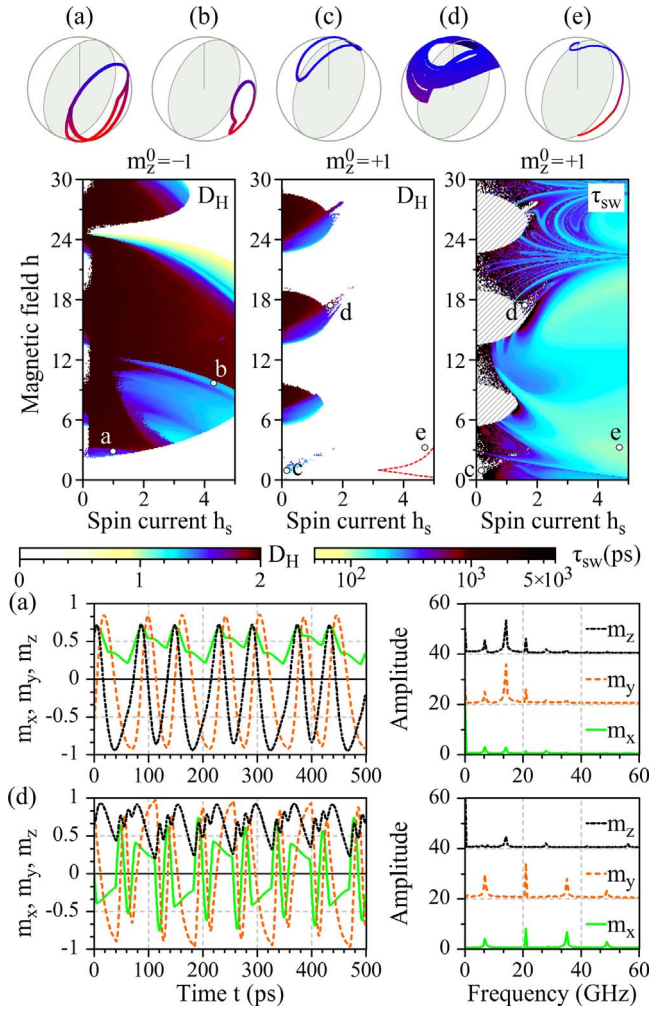

FIG. 13. (Color online) Synchronization diagram for the macrospin subject to the square-shaped microwave with the frequency $f_h=14$ GHz. Characteristic phase portraits are the following: (a) $h_s=1$, $h=2.9$; (b) $h_s=4.3$, $h=9.7$; (c) $h_s=0.17$, $h=0.95$; (d) $h_s=1.6$, $h=17.45$; (e) $h_s=4.7$, $h=3.25$. The dashed-line contour in the central panel denotes the BMR area.

pulse sequence is favorable for switching the macrospin dynamics between several motion types depending on the current magnetization orientation, causing pronounced kinks on the phase portraits like those seen in Fig. 12(a). For weaker fields one obtains hybrid cycles like, for example, two merged OPP loops of different curvature [Fig. 12(b)]. The large synchronization island in the left panel of Fig. 12 yields complex magnetization oscillations around the canted state axis forming multiple loops of different radii like those shown in Fig. 12(c). Magnetization reversal also becomes affected by the abrupt periodic changes of the field. In particular, the phase portrait shown in Fig. 12(d) exhibits distinct dynamics for each pulse occurring during its formation. The first pulse "kicks" the magnetization from the equilibrium state toward the lower hemisphere via gradual precession, eventually drawing it into the attraction basin of an OPP cycle. As soon as the pulse switches off, the macrospin starts precession along the small-amplitude OPP trajectory, and the next pulse concludes the switching process. Such multistage reversals is characterized by larger switching time ($\tau_{sw}\approx 250$ ps). Naturally, macrospin switching attainable in the expanded BMR region is much lower ($\tau_{sw}\approx 130$ ps), yielding the phase trajectory that almost precisely traces the meridian corresponding to the easy magnetization plane [Fig. 12(e)], without any ringing effects.

For $f_h=14$ GHz, the synchronization areas become larger (Fig. 13). In particular, the time series for magnetization components of the phase portrait shown in Fig. 13(a) allow to discern the parts belonging to individual OPP cycles in the m_x plot. Previously discussed superposition of two OPP cycles features much more regular form and larger amplitude [Fig. 13(b)]. For initial magnetization $m_z^0\approx +1$, it is possible to obtain narrow-angle precession around the easy axis at weak field [Fig. 13(c)]. For higher h the oscillations become noisy, featuring characteristic jumps of m_x and m_y [Fig. 13(d), see also the bottom panel] reflected by sharp peaks of frequency about 21 GHz. The oscillations of m_z represent a saw-tooth signal, which can be measured experimentally and can be used as a converter of incoming square-shaped magnetization pulses into triangular ones. The shortest switching time observed in the system is $\tau_{sw}=107$ ps for the phase portrait shown in Fig. 13(e).

E. Effect of field frequency and amplitude on macrospin dynamics

To investigate the effect of field oscillation frequency on the macrospin dynamics for different profiles of the field pulses we calculated the diagrams $D_H(f_h,h)$ for the case of $h_s=0$ (Fig. 14). As we see from this figure, for the harmonic pulses (upper panel in the figure) the diagram consists of the series of the round-shaped islands, outside which the system cannot leave the equilibrium state. The width of these islands changes in a nonlinear way with f_h. The increase in frequency beyond 30–40 GHz results in zero D_H. Inside the islands the system can be either synchronized (light areas) or not synchronized with the microwave (dark areas). It is worth emphasizing that the boundary between these regions is usually blurred and noisy. For lower frequencies, the fine tuning allows to get the phase portrait representing a superposition of IPP and OPP cycles [Figs. 14(a)–14(c)]. Upon increase of the cycle loop number, one can observe the frequency increase for the magnetization oscillations generated by a macrospin. We were able to record the frequencies reaching 40 GHz for the m_y component [Fig. 15(c)], which is about 2000% increase in the driving force frequency $f_h=2.2$ GHz. Even though the m_y component cannot be directly measured by GMR, these high-frequency oscillations can be experimentally found rotating the phase portrait around the axis perpendicular to the easy plane upon the application of a tilted magnetic field.[49] For larger pulse frequencies the synchronization areas within the islands become wider, and the phase portraits of the magnetization precession are simpler. In particular, for the fields $h\approx 8$ and $f_h\approx 9$ GHz it is possible to get two coupled OPP cycles [Fig. 14(f)]. Another island accessible at higher frequencies features single OPP cycles [Fig. 14(d)] for applied fields of $0<h<20$ and frequencies $f_h>8$. Close to the darker bands

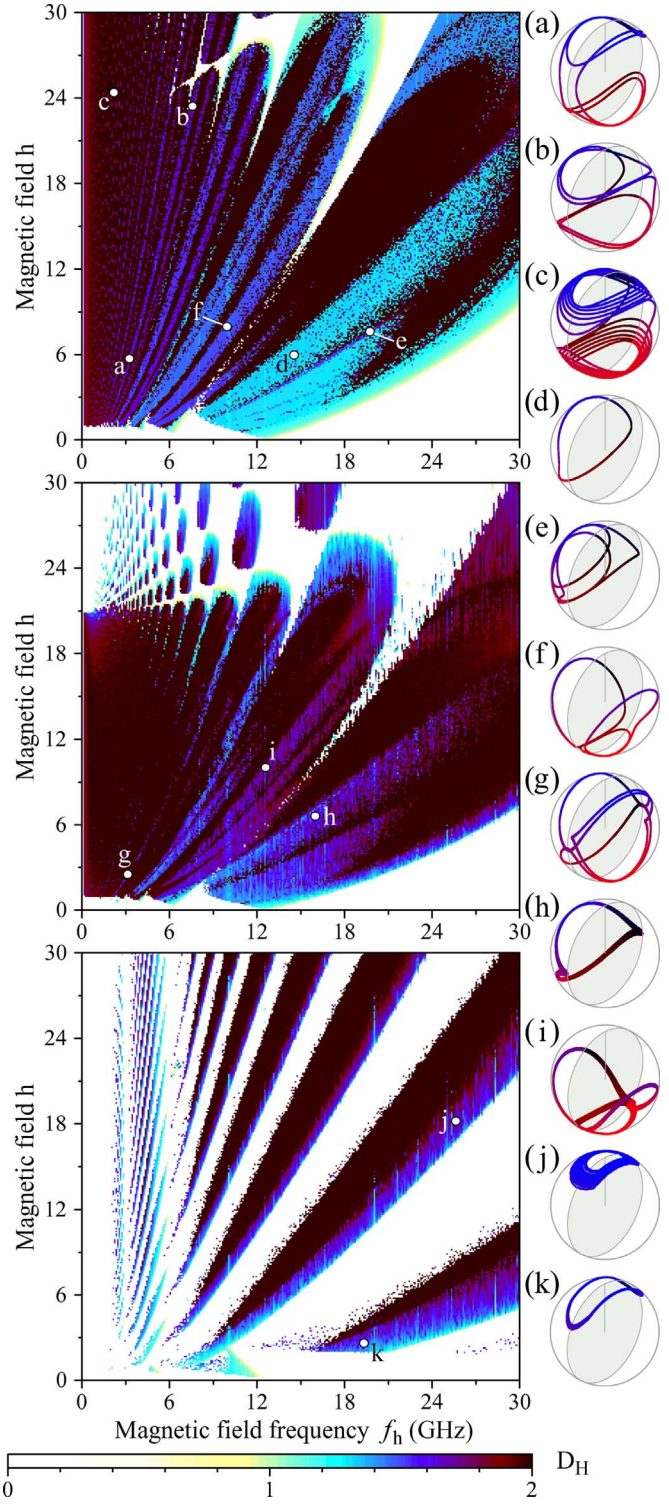

FIG. 14. (Color online) Synchronization diagrams for harmonic h^H (top panel), signed square h^S (middle panel), and unsigned square h^U (bottom panel) field pulses calculated for the case when no spin current is injected, h_s=0. Characteristic phase portraits are the following: (a) f_h=3.25 GHz, h=5.7; (b) f_h=7.6 GHz, h=23.45; (c) f_h=2.2 GHz, h=24.4; (d) f_h=14.55 GHz, h=5.95; (e) f_h=19.75 GHz, h=7.6; (f) f_h=9.95 GHz, h=7.95; (g) f_h=3.15 GHz, h=2.5; (h) f_h=16 GHz, h=6.5; (i) f_h=12.6 GHz, h=10; (j) f_h=25.65 GHz, h=18.2; (k) f_h=19.35 GHz, h=2.6.

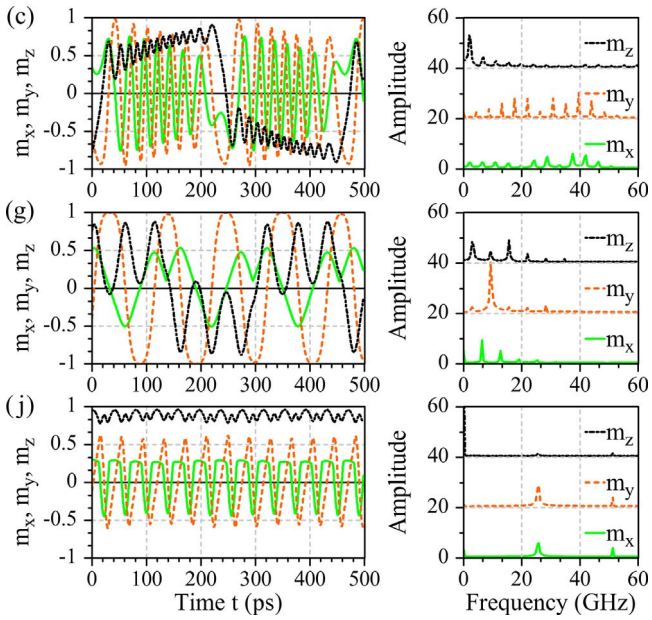

FIG. 15. (Color online) Time dependence of individual magnetization components for the phase portraits shown in Fig. 14 with the corresponding FFT spectra.

within the islands the system gradually loses its synchronization so that the phase portrait gains additional loops [Fig. 14(e)].

The middle panel of Fig. 14 shows the corresponding macrospin dynamics calculated for the case of signed square-shaped field pulses h^S. The "island-structure" of the diagram is still clearly discernible, but due to less convenient control inferred by the rectangular field pulses, the overall macrospin synchronization is significantly lower and phase portraits are blurred causing higher D_H values (i.e., darker tone in the figure). Moreover, for higher fields the islands become detached, increasing the areas in the parameter space for which the system cannot be moved out of the equilibrium. To compare with the harmonic pulses, we presented the phase portraits calculated for topologically similar positions in the synchronization diagram, as those shown in the top panel. One can see that a general shape of the phase trajectory for the square pulses becomes less smooth and features sharp kinks [compare, for example, the phase trajectories shown in Fig. 14(g) and 14(a)]. At the same time, under square pulses the amplitude of the m_z oscillations within the signal packets becomes larger [compare Fig. 15(g) to Fig. 15(c)], which increases the chance that such oscillations can be experimentally detected. Joined OPP cycles similar to those shown in Fig. 14(f) become significantly noisy [Fig. 14(i)] if being triggered by signed square field pulses. Even a single OPP cycle appears to be distorted [Fig. 14(h)].

The application of unsigned square pulses to the system renders completely different macrospin response (Fig. 14, bottom panel), transforming the islands on the synchronization diagram into the series of dark-colored bands signaling the absence of synchronization. At the boundary of these bands, one obtains closed noisy magnetization trajectories [Fig. 14(j)]. A "cleaner" version of the same phase portrait is available under weak fields ($h \lesssim 6$) and large oscillation fre-

quencies [Fig. 14(k)]. The time evolution of the individual magnetization components [Fig. 14(j)] reveals that the discussed type of the phase portrait is characterized by abrupt pulses of m_x and saw-tooth oscillations of m_y. Such sharp magnetization oscillation profiles could also be of interest for applications.

Therefore, to obtain the periodic magnetization motion generated by the field pulses with the purpose of using the magnetization oscillations of GHz frequency detectable by GMR, one should use the harmonically varied magnetic field. Even if the formation of the signed square-shaped field pulses could be achieved with less significant experimental efforts, the resulting oscillations are noisier and thus less usable. The number of states in $[h, f_h]$ parameter space to which the field will fail to drive the macrospin out of the equilibrium would increase significantly. Finally, use of unsigned square shape of the field oscillations would yield even more limitations, featuring a much smaller variety of possible oscillation types and a significantly increased area where the macrospin keeps its initial orientation.

V. CONCLUSIONS

Numerical simulations of the macrospin dynamics with the Landau-Lifshitz-Gilbert equation using the generalized form of the viscous damping coefficient, as proposed by Tiberkevich and Slavin,[47] allowed to achieve several important results on macrospin magnetization dynamics, using the model of a ferromagnet with the parameters of Co and the dimensions which are commonly used in spin valve experiments.

By injecting the spin current with a polarization collinear with the easy axis it is possible to realize the magnetization reversal by one single pulse, achieving the fastest switching time $\tau_{sw} \simeq 200$ ps for the ballistic trajectory. Magnetization reversal can be performed with shorter pulses, if higher currents are applied; multiple pulses enables significant expansion of the frequency/pulse length ranges, for which the magnetization reversal can be accomplished. Moreover, the magnetization switching time plotted as a function of spin current features a set of pronounced plateaus, allowing to obtain the same τ_{sw} for significantly wide ranges of h_s values.

For the case when the magnetization switching is obtained by the time-variable field, the multiple square-shaped pulses allow to reach the switching time of about 100 ps, approaching the fundamental limit of the field-induced magnetization reversal. Our numerical simulations revealed the presence of a wedge-shaped area in $[h_s, h]$ parameter space, where magnetization reversal follows the ballistic trajectory passing in the vicinity of the easy magnetization plane, practically without any ringing. It was shown that both the shape and size of this area can be controlled by changing the time profile and the frequency of applied field pulses, allowing to predict the ranges of external parameters required to obtain efficient low-field magnetization reversal along the shortest possible trajectory. In general, the minimization of switching time requires simultaneous adjustment of the field amplitude, frequency, and the density of injected spin current. Here, the role of temperature is not addressed. As shown recently however using a similar method,[32] for thermal energies below the anisotropy energy the qualitative features of the spin dynamics remain intact.

In view of exploiting spintronic devices for the generation of GHz magnetic oscillations, the most important role appears to belong to the proper choice of the shapes of the field pulses. We found that the most promising oscillation modes can be obtained by using harmonic field oscillations, allowing to get the multiplication of the oscillation frequency when no spin current is injected to the system. The same oscillation mode transforms the harmonic control pulse to a set of high-frequency oscillation "packets," which can be useful for the modulators of an incoming signal. In contrast, the square-shaped sign-varying pulses of magnetic field are much less practical, leading to noise and to the appearance of kinks on the phase trajectories. The unsigned square pulses of the magnetic field create less variety of the synchronized phase states, but enable the periodic oscillations with saw-tooth temporal distribution of the macrospin projection.

In conclusion, for the considered geometry and material parameters, the use of unsigned square-shaped pulses of both spin current and magnetic field is the most effective way to achieve fast magnetization reversal, even by means of a single pulse. For the generation of periodic magnetization oscillations of GHz frequency, the best option is to use harmonically alternating magnetic fields.

ACKNOWLEDGMENTS

This work was partially supported by FCT Grants Nos. POCI/FIS/58746/2004 and SFRH/BPD/26825/2006 in Portugal, by the STCU Grant No. 3098 in Ukraine, and by funds of the Polish Ministry of Science and Higher Education as research projects in years 2006–2009 and 2007–2010.

*Permanent position: Department of Physics, Adam Mickiewicz University, Umultowska 85, 61-614 Poznań, Poland.

[1] J. A. Katine, F. J. Albert, R. A. Buhrman, E. B. Myers, and D. C. Ralph, Phys. Rev. Lett. **84**, 3149 (2000).

[2] S. I. Kiselev, J. C. Sankey, I. N. Krivorotov, N. C. Emley, R. J. Schoelkopf, R. A. Buhrman, and D. C. Ralph, Nature (London) **425**, 380 (2003).

[3] S. I. Kiselev, J. C. Sankey, I. N. Krivorotov, N. C. Emley, M. Rinkoski, C. Perez, R. A. Buhrman, and D. C. Ralph, Phys. Rev. Lett. **93**, 036601 (2004).

[4] Hiaven Xi, Kai-Zhong Gao, and Yiming Shi, Appl. Phys. Lett. **84**, 4977 (2004).

[5] S. Kaka, M. R. Pufall, W. H. Rippard, T. J. Silva, S. E. Russek, and J. A. Katine, Nature (London) **437**, 389 (2005).

[6] S. I. Kiselev, J. C. Sankey, I. N. Krivorotov, N. C. Emley, A. G. F. Garcia, R. A. Buhrman, and D. C. Ralph, Phys. Rev. B **72**, 064430 (2005).
[7] M. N. Baibich, J. M. Broto, A. Fert, F. Nguyen Van Dau, F. Petroff, P. Eitenne, G. Creuzet, A. Friederich, and J. Chazelas, Phys. Rev. Lett. **61**, 2472 (1988).
[8] J. Z. Sun, Phys. Rev. B **62**, 570 (2000).
[9] J. Xiao, A. Zangwill, and M. D. Stiles, Phys. Rev. B **72**, 014446 (2005).
[10] M. D. Stiles and J. Miltat, in *Spin Dynamics in Confined Magnetic Structures III: Topics in Applied Physics*, edited by B. Hillebrands and A. Thiaville (Springer, Berlin, 2006), Vol. 101.
[11] T. Devolder and C. Chappert, Eur. Phys. J. B **36**, 57 (2003).
[12] Ya. B. Bazaliy, B. A. Jones, and Shou-Cheng Zhang, Phys. Rev. B **69**, 094421 (2004).
[13] M. Bauer, R. Lopusnik, J. Fassbender, B. Hillerbrands, J. Bangert, and J. Wecker, J. Appl. Phys. **91**, 543 (2002).
[14] G. Finocchio, I. Krivorotov, M. Carpentieri, G. Consolo, B. Azzerboni, L. Torres, E. Martinez, and L. Lopez-Diaz, J. Appl. Phys. **99**, 08G507 (2006).
[15] J. Fransson, Phys. Rev. B **77**, 205316 (2008).
[16] H. Morise and S. Nakamura, J. Magn. Magn. Mater. **306**, 260 (2006).
[17] J. Sun, Nature (London) **425**, 359 (2003).
[18] A. Canizo-Cabrera, V. Garcia-Vazquez, and Te-ho Wu, J. Appl. Phys. **99**, 08G512 (2006).
[19] F. J. Albert, N. C. Emley, E. B. Myers, D. C. Ralph, and R. A. Buhrman, Phys. Rev. Lett. **89**, 226802 (2002).
[20] Q. F. Xiao, B. C. Choi, J. Rudge, Y. K. Hong, and G. Donohoe, J. Appl. Phys. **101**, 024306 (2007).
[21] H. W. Schumacher, S. Serrano-Guisan, K. Rott, and G. Reiss, Appl. Phys. Lett. **90**, 042504 (2007).
[22] H. W. Schumacher, C. Chappert, R. C. Sousa, and P. P. Freitas, Appl. Phys. Lett. **83**, 2205 (2003).
[23] Di Xiao, M. Tsoi, and Qian Niu, J. Appl. Phys. **99**, 013903 (2006).
[24] C. Thirion, W. Wernsdorfer, and D. Mailly, Nat. Mater. **2**, 524 (2003).
[25] L. Thomas, M. Hayashi, X. Jiang, R. Moriya, C. Rettner, and S. Parkin, Science **315**, 1553 (2007).
[26] K. Rivkin and J. B. Ketterson, Appl. Phys. Lett. **88**, 192515 (2006).
[27] K. Rivkin and J. B. Ketterson, Appl. Phys. Lett. **89**, 252507 (2006).
[28] H. W. Schumacher, C. Chappert, R. C. Sousa, P. P. Freitas, and J. Miltat, Phys. Rev. Lett. **90**, 017204 (2003).
[29] L. He and W. D. Doyle, J. Appl. Phys. **79**, 6489 (1996).
[30] Z. Z. Sun and X. R. Wang, Phys. Rev. B **73**, 092416 (2006).
[31] Z. Z. Sun and X. R. Wang, Phys. Rev. Lett. **97**, 077205 (2006).
[32] A. Sukhov and J. Berakdar, J. Phys.: Condens. Matter **20**, 125226 (2008).
[33] P. Podio-Guidugli and G. Tomassetti, IEEE Trans. Magn. **42**, 3652 (2006).
[34] M. Belmeguenai, T. Devolder, and C. Chappert, J. Phys. D **39**, 1 (2006).
[35] Z. Z. Sun and X. R. Wang, Phys. Rev. B **74**, 132401 (2006).
[36] G. Bertotti, A. Magni, I. D. Meyerdgoyz, and C. Serpico, J. Appl. Phys. **89**, 6710 (2001).
[37] Z. Li, Y. C. Li, and S. Zhang, Phys. Rev. B **74**, 054417 (2006).
[38] P. M. Gorley, P. P. Horley, V. K. Dugaev, J. Barnaś, and W. Dobrowolski, J. Appl. Phys. **101**, 034504 (2007).
[39] T. L. Gilbert, IEEE Trans. Magn. **40**, 3443 (2004).
[40] H. Katsura, A. V. Balatsky, Z. Nussinov, and N. Nagaosa, Phys. Rev. B **73**, 212501 (2006).
[41] W. J. Kim, T. D. Lee, and K. J. Lee, IEEE Trans. Magn. **42**, 3207 (2006).
[42] Ya. Tserkovnyak, A. Brataas, and G. E. W. Bauer, Phys. Rev. Lett. **88**, 117601 (2002).
[43] K. Lenz, H. Wende, W. Kuch, K. Baberschke, K. Nagy, and A. Jánossy, Phys. Rev. B **73**, 144424 (2006).
[44] S. Karakurt, R. W. Chantrell, and U. Nowak, J. Magn. Magn. Mater. **316**, e280 (2007).
[45] D. L. Mills and R. Arias, Physica B (Amsterdam) **384**, 147 (2006).
[46] J. Lee, D. Suess, T. Schrefl, K. Hwan Oh, and J. Fidler, IEEE Trans. Magn. **42**, 3210 (2006).
[47] V. Tiberkevich and A. Slavin, Phys. Rev. B **75**, 014440 (2007).
[48] V. V. Gorley and V. A. Shenderovskiy, Zh. Tekh. Fiz. **51**, 13 (1981).
[49] P. P. Horley, V. R. Vieira, P. M. Gorley, V. K. Dugaev, and J. Barnaś, Phys. Rev. B **77**, 094427 (2008).
[50] G. Bertotti, I. D. Meyergoyz, and C. Serpico, J. Appl. Phys. **91**, 7556 (2002).
[51] A. J. Lichtenberg and M. A. Lieberman, *Regular and Stochastic Dynamics* (Springer, New York, 1992).
[52] T. Devolder, C. Chappert, J. A. Katine, M. J. Carey, and K. Ito, Phys. Rev. B **75**, 064402 (2007).
[53] Z. Z. Sun and X. R. Wang, Phys. Rev. B **71**, 174430 (2005).
[54] Z. Yang, S. Zhang, and Y. C. Li, Phys. Rev. Lett. **99**, 134101 (2007).